A Mixed Multiscale FEM for the Eddy-Current Problem With T, Φ–Φ in Laminated Conducting Media

Karl Hollaus and Markus Schöbinger

Institute for Analysis and Scientific Computing, Vienna University of Technology (TU Wien), A-1040 Vienna, Austria

A novel mixed multiscale finite-element method for the eddy-current problem is presented to avoid the necessity of modeling each laminate of the core of electrical devices. The method is based on a current vector potential T and a reduced magnetic scalar potential (RMSP) Φ and copes with the 3-D problems. The edge effect is considered. Material properties are assumed to be linear. Hence, the method is developed for the frequency domain. External currents are represented by the Biot–Savart field serving as excitation. The planes of symmetry are exploited. Numerical simulations are presented, showing excellent accuracy at minimal computational costs.

Index Terms— **Biot–Savart field, current vector potential (CVP), eddy-current problem (ECP), laminated media, mixed multiscale finite-element method (MMSFEM), reduced magnetic scalar potential (RMSP).**

I. Introduction

AN ACCURATE prediction of the eddy-current distribution in the laminated iron cores of electric devices is a challenging task in the design process. Modeling of each laminate requires many finite elements, leading to extremely large equation systems. The computational costs to solve these systems are prohibitively high.

The solution obtained by prescribing a current vector potential (CVP) $\boldsymbol{T}$ having a single component normal to the lamination [1] or using an anisotropic electric conductivity [2] has to be corrected in a post-processing step to consider the eddy currents due to the main magnetic flux. These approaches are questionable in the context of nonlinear material properties. Multiscale finite-element methods (MSFEMs) provide the solution in one step taking account of both magnetic stray flux perpendicular to the lamination and main magnetic flux parallel to the lamination.

The capacity of the MSFEMs is well known [3]. An MSFEM in 3-D for eddy currents in laminated iron cores based on the magnetic vector potential $\boldsymbol{A}$ has been presented in [4] recently. A CVP $\boldsymbol{T}$ [5] with a reduced magnetic scalar potential (RMSP) Φ can also be used for an eddy-current problem (ECP) [6], [7]. The $\boldsymbol{T}$, Φ–Φ formulation is popular to simulate the eddy currents, for instance, in the core of transformers.

Often 2-D/1-D-methods are used to simulate the electrical machines. These methods are based on the assumption that the influence of the magnetic stray fields in the end region of the electrical machines can be neglected. This means that each laminate is exposed to the same electromagnetic field distribution, and therefore, a simulation of a single laminate suffices [8], [9]. Such problems are solved elegantly with 2-D/1-D-MSFEMs [10]. However, this kind of methods is not in the scope of this article.

Manuscript received August 19, 2019; revised November 6, 2019; accepted November 12, 2019. Date of publication January 13, 2020; date of current version March 18, 2020. Corresponding author: K. Hollaus (e-mail: karl.hollaus@tuwien.ac.at).

Color versions of one or more of the figures in this article are available online at http://ieeexplore.ieee.org.

Digital Object Identifier 10.1109/TMAG.2019.2954480

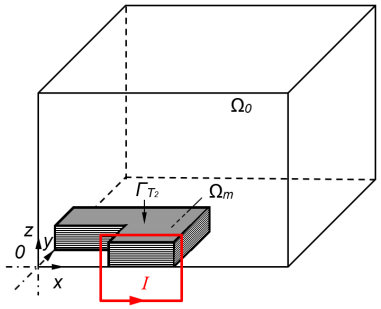

Fig. 1. ECP with a laminated core (gray) and a filamentary current (red) excites the problem, and O is the origin at (0, 0, 0). The planes of symmetry are $x = 0$: Γ_{H_c} and Γ_{H_0}, $y = 0$: Γ_{H_c} and Γ_{H_0}, and $z = 0$: Γ_B and Γ_E. Far boundary: Γ_{H_0}. For details, see also Sections II-B and IV-A.

The magnetic-flux density parallel to the lamination is expanded into orthogonal even polynomials, the so-called skin-effect sub-basis functions, to improve the local approximation in [11]. A higher order multiscale expansion of electromagnetic field problems exploiting a single component CVP can be found in [12]. A mixed MSFEM (MMSFEM) based on the magnetic vector potential $\boldsymbol{A}$ and the current density $\boldsymbol{J}$ has been developed in [3] to take account of the edge effect in particular.

The construction of the mixed multiscale approach for the novel MMSFEM is presented. Eddy-current losses obtained by the MMSFEM have been compared with those obtained by reference solutions of finite-element models considering each laminate. Numerical examples, as shown in Fig. 1, have been studied to show the very satisfactory performance of the MMSFEM with respect to accuracy and computational costs.

II. T, Φ–Φ Formulation

The $\boldsymbol{T}$, Φ–Φ formulation is introduced extremely shortened, and the associated boundary value problem along with the weak form for eddy currents is summarized in the following.

A. T, Φ–Φ Formulation

Considering Ampere's law $\operatorname{curl} \boldsymbol{H} = \boldsymbol{J} + \boldsymbol{J}_0$ with an impressed current density $\boldsymbol{J}_0$, the magnetic-field strength

$$\boldsymbol{H} = \boldsymbol{T} + \boldsymbol{T}_{\mathrm{BS}} - \operatorname{grad} \Phi \tag{1}$$

in the conducting domain Ω_c can be represented by a CVP $\boldsymbol{T}$ and an RMSP Φ, where $\boldsymbol{J}_0$ is replaced by its Biot–Savart field $\boldsymbol{T}_{\mathrm{BS}}$. The potentials $\boldsymbol{T}$ and Φ describe the quasi-static magnetic field in Ω_c. The static magnetic field in the non-conducting domain Ω_0 can be written as

$$\boldsymbol{H} = \boldsymbol{T}_{\mathrm{BS}} - \operatorname{grad}\Phi. \tag{2}$$

B. Boundary Value Problem With $\boldsymbol{T}$, Φ–Φ

The ECP to be solved in this article is sketched in Fig. 1. It consists of laminates Ω_c enclosed by air Ω_0, $\Omega = \Omega_c \cup \Omega_0$. The laminated domain Ω_m used by the MMSFEM consists of the conducting laminates Ω_c and the insulation layers in between.

Thus, the following boundary value problem for the $\boldsymbol{T}$, Φ–Φ formulation is obtained [7].

The quasi-static magnetic field in the conducting domain Ω_c

$$\begin{aligned}
\operatorname{curl}(\rho \operatorname{curl}\boldsymbol{T}) + j\omega\mu\boldsymbol{T} - j\omega\mu \operatorname{grad}\Phi \\
= -\operatorname{curl}(\rho \operatorname{curl}\boldsymbol{T}_{\mathrm{BS}}) - j\omega\mu\boldsymbol{T}_{\mathrm{BS}} \qquad (3)\\
j\omega \operatorname{div}(\mu\boldsymbol{T} - \mu \operatorname{grad}\Phi) = -j\omega \operatorname{div}(\mu\boldsymbol{T}_{\mathrm{BS}}) \quad \text{in } \Omega_c \qquad (4)\\
\rho \operatorname{curl}\boldsymbol{T} \times \boldsymbol{n} = -\rho \operatorname{curl}\boldsymbol{T}_{\mathrm{BS}} \times \boldsymbol{n} \qquad (5)\\
\mu(\boldsymbol{T} - \operatorname{grad}\Phi)\cdot\boldsymbol{n} = -\mu\boldsymbol{T}_{\mathrm{BS}}\cdot\boldsymbol{n} \quad \text{on } \Gamma_E \qquad (6)\\
\boldsymbol{T} \times \boldsymbol{n} = -\boldsymbol{T}_{\mathrm{BS}} \times \boldsymbol{n}\ (=\boldsymbol{0}) \qquad (7)\\
\Phi = \Phi_0\ (=0) \quad \text{on } \Gamma_{H_c}. \qquad (8)
\end{aligned}$$

The static magnetic field in the non-conducting domain Ω_0

$$\begin{aligned}
-j\omega \operatorname{div}(\mu \operatorname{grad}\Phi) = -j\omega \operatorname{div}(\mu\boldsymbol{T}_{\mathrm{BS}}) \quad \text{in } \Omega_0 \qquad (9)\\
-\boldsymbol{n}\cdot\mu \operatorname{grad}\Phi = b - \boldsymbol{n}\cdot\mu\boldsymbol{T}_{\mathrm{BS}} \quad \text{on } \Gamma_B \qquad (10)\\
\Phi = \Phi_0\ (=0) \quad \text{on } \Gamma_{H_0}. \qquad (11)
\end{aligned}$$

The interface (between Ω_c and Ω_0) condition on Γ_{c0}

$$\boldsymbol{T} \times \boldsymbol{n} = \boldsymbol{0} \quad \text{on } \Gamma_{c0}. \tag{12}$$

Indices E, H, or B mean that the tangential components of E and H or the normal component of B are prescribed, and in addition, c and 0 denote the surfaces, which are the boundaries of Ω_c and Ω_0, respectively. The material parameters are the magnetic permeability μ and the electric resistivity ρ, respectively, j denotes the imaginary unit, ω is the angular frequency, and $\boldsymbol{n}$ is the normal unit vector on a surface pointing outward of the respective domain.

C. Weak Form With $\boldsymbol{T}$, Φ–Φ

The weak form for the finite-element method is as follows.

Find $(\boldsymbol{T}_h, \Phi_h) \in V_{Dh} := \{(\boldsymbol{T}_h, \Phi_h) : \boldsymbol{T}_h \in \mathcal{U}_h, \Phi_h \in \mathcal{V}_h$ and $\boldsymbol{T}_h \times \boldsymbol{n} = -\boldsymbol{T}_{\mathrm{BS}} \times \boldsymbol{n}\ (=\boldsymbol{0})$ on $\Gamma_{0c} \cup \Gamma_{H_c}$, $\Phi_h = \Phi_0\ (=0)$ on $\Gamma_{H_c} \cup \Gamma_{H_0}\}$, such that

$$\begin{aligned}
&\int_{\Omega_c} \rho \operatorname{curl}\boldsymbol{T}_h \cdot \operatorname{curl}\boldsymbol{v}_h \, d\Omega + j\omega \int_{\Omega_c} \mu(\boldsymbol{T}_h - \operatorname{grad}\Phi_h)\cdot\boldsymbol{v}_h \, d\Omega \\
&= -\int_{\Omega_c} \rho \operatorname{curl}\boldsymbol{T}_{\mathrm{BS}h} \cdot \operatorname{curl}\boldsymbol{v}_h \, d\Omega - j\omega \int_{\Omega_c} \mu\boldsymbol{T}_{\mathrm{BS}h}\cdot\boldsymbol{v}_h \, d\Omega
\end{aligned} \tag{13}$$

$$\begin{aligned}
&j\omega \int_{\Omega} \mu \operatorname{grad}\Phi_h \cdot \operatorname{grad}\upsilon_h \, d\Omega - j\omega \int_{\Omega_c} \mu\boldsymbol{T}_h \cdot \operatorname{grad}\upsilon_h \, d\Omega \\
&= j\omega \int_{\Omega} \mu\boldsymbol{T}_{\mathrm{BS}h} \cdot \operatorname{grad}\upsilon_h \, d\Omega - j\omega \int_{\Gamma_B} b_h\upsilon_h \, d\Gamma
\end{aligned} \tag{14}$$

for all $(\boldsymbol{v}_h, \upsilon_h) \in V_{0h}$, where $\mathcal{U}_h$ and $\mathcal{V}_h$ are the finite-element subspaces of $H(\operatorname{curl}, \Omega_c)$ and $H^1(\Omega)$, respectively.

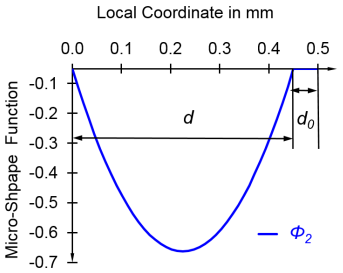

Fig. 2. Micro-shape function ϕ_2.

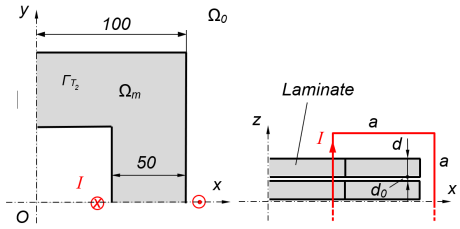

Fig. 3. Numerical example, problem not drawn to scale, origin O at (0, 0, 0), $x = 0$, $y = 0$, and $z = 0$ represents the planes of symmetry. Top view (left) and front view (right) of one-eighth with four laminates (dimensions are in mm), and the structure is quadratic in the xy plane; quadratic filamentary current: $a = 70$ mm and arranged symmetric with respect to the cross section of the limb.

III. Mixed Multiscale Finite-Element Method

A. Mixed Multiscale Approach for $\boldsymbol{T}$, Φ–Φ

Multiscale approaches are based on the fact that the problem can be observed on the large scale with the overall dimensions of the laminated core, on the one hand, and, on the other, on the small scale with the very small thickness of the laminates d and the width of the insulation layer d_0 in between (see Fig. 3). Thus, it would be obvious to assume the mixed multiscale approach

$$\widetilde{\boldsymbol{T}} = \boldsymbol{T}_0 + \phi_2\boldsymbol{T}_2 \tag{15}$$

$$\widetilde{\Phi} = \Phi_0 + \phi_2\Phi_2 \tag{16}$$

where the mean values $\boldsymbol{T}_0$ and Φ_0 consider the large-scale variation of the solution and $\boldsymbol{T}_2$ and Φ_2 with the even periodic micro-shape function ϕ_2 (see Fig. 2), the highly oscillating variation of the solution on the small scale.

Therefore, the magnetic field represented in (1) and (2) could now be written as

$$\widetilde{\boldsymbol{H}} = \boldsymbol{T}_0 + \boldsymbol{T}_2\phi_2 + \boldsymbol{T}_{\mathrm{BS}} - \operatorname{grad}\Phi_0 - \operatorname{grad}(\Phi_2\phi_2) \quad \text{in } \Omega_m \tag{17}$$

$$\widetilde{\boldsymbol{H}} = \boldsymbol{T}_{\mathrm{BS}} - \operatorname{grad}\Phi_0 \quad \text{in } \Omega_0. \tag{18}$$

However, investigations and considerations led to the understanding that Φ_0 copes with the perturbation of the overall field due to the laminated core and $\boldsymbol{T}_0$ can be omitted. On the other hand, $\operatorname{grad}(\Phi_2\phi_2)$ has also been neglected, because it is supported by the irrotational part of $\phi_2\boldsymbol{T}_2$ as well as an odd periodic magnetic field is not expected for the considered problem in Fig. 3. These assumptions are well substantiated by the numerical results in Section IV-B.

That is why the simplified mixed multiscale approach

$$\widetilde{\boldsymbol{T}} = \boldsymbol{T}_2\phi_2 \tag{19}$$

$$\widetilde{\Phi} = \Phi_0 \tag{20}$$

has been used in this article. Thus, the magnetic field in (17) and (18), respectively, can be written for the MMSFEM

$$\widetilde{\boldsymbol{H}} = \boldsymbol{T}_{\mathrm{BS}} + \boldsymbol{T}_2\phi_2 - \operatorname{grad}\Phi_0 \quad \text{in } \Omega_m \tag{21}$$

and

$$\widetilde{\boldsymbol{H}} = \boldsymbol{T}_{\mathrm{BS}} - \operatorname{grad}\Phi_0 \quad \text{in } \Omega_0. \tag{22}$$

B. Weak Form for $\widetilde{\boldsymbol{T}}$, $\widetilde{\Phi}$–$\widetilde{\Phi}$

The weak form for the MMSFEM reads as follows.

Find $(\boldsymbol{T}_{2h}, \Phi_{0h}) \in V_{Dh} := \{(\boldsymbol{T}_{2h}, \Phi_{0h}) : \boldsymbol{T}_{2h} \in \mathcal{U}_h, \Phi_{0h} \in \mathcal{V}_h$ and $\boldsymbol{T}_{2h} \times \boldsymbol{n} = \boldsymbol{0}$ on $\Gamma_{m0} \setminus \Gamma_{T_2} \cup \Gamma_{H_c}$, $\Phi_{0h} = \Phi_0\ (=0)$ on $\Gamma_{H_c} \cup \Gamma_{H_0}\}$, such that

$$\begin{aligned}
&\int_{\Omega_c} \rho \operatorname{curl}(\boldsymbol{T}_{2h}\phi_2) \cdot \operatorname{curl}(\boldsymbol{v}_{2h}\phi_2)\, d\Omega \\
&\qquad + j\omega \int_{\Omega_c} \mu(\boldsymbol{T}_{2h}\phi_2 - \operatorname{grad}\Phi_{0h}) \cdot \boldsymbol{v}_{2h}\phi_2\, d\Omega \\
&\quad = -\int_{\Omega_c} \rho \operatorname{curl} \boldsymbol{T}_{\mathrm{BS}h} \cdot \operatorname{curl}(\boldsymbol{v}_{2h}\phi_2)\, d\Omega \\
&\qquad - j\omega \int_{\Omega_c} \mu \boldsymbol{T}_{\mathrm{BS}h} \cdot \boldsymbol{v}_{2h}\phi_2\, d\Omega
\end{aligned} \tag{23}$$

$$\begin{aligned}
&j\omega \int_{\Omega} \mu \operatorname{grad}\Phi_{0h} \cdot \operatorname{grad} v_{0h}\ d\Omega \\
&\qquad - j\omega \int_{\Omega_c} \mu \boldsymbol{T}_{2h}\phi_2 \cdot \operatorname{grad} v_{0h} d\Omega \\
&\quad = j\omega \int_{\Omega} \mu \boldsymbol{T}_{\mathrm{BS}h} \cdot \operatorname{grad} v_{0h}\ d\Omega - j\omega \int_{\Gamma_B} b_h v_{0h}\ d\Gamma
\end{aligned} \tag{24}$$

for all $(\boldsymbol{v}_{2h}, v_{0h}) \in V_{0h}$, where $\mathcal{U}_h \subset H(\operatorname{curl}, \Omega_m)$, $\mathcal{V}_h \subset H^1(\Omega)$, and $\phi_2 \in H^1_{\mathrm{per}}(\Omega_m)$ have been selected.

The interface between Ω_m and Ω_0 is denoted by Γ_{m0} and Γ_{T_2} is the part of Γ_{m0}, which represents the smooth surface of the laminated core, compared with Figs. 1 and 3. The arising coefficients in (23) and (24) have been averaged, as demonstrated in [3]. Since the micro-shape function ϕ_2 is the even function shown in Fig. 2 with respect to the center of the laminate, the highly oscillating second term on the RHS in (23) does not vanish.

IV. Numerical Simulations

A. Numerical Problems

Problems consisting of different numbers of laminates have been investigated, compared with Fig. 3. The thickness of the laminates and an unfavorable width of the insulation layers have been selected with $d = 0.45$ mm and $d_0 = 0.05$ mm. A conductivity of $\sigma = 2 \times 10^6$ S/m and a relative permeability of $\mu_r = 1000$ have been assumed. For the sake of simplicity, the filamentary current was selected to deal easily with the linear forms on the right-hand sides of the weak form in (23) and (24). The rectangular filamentary current generates the Biot–Savart field $\boldsymbol{T}_{\mathrm{BS}}$, which serves as a source field. Each straight segment of the rectangular loops has been split into four sub-segments. Gauss integration with three integration points was used to approximate

$$\boldsymbol{T}_{\mathrm{BS}h} = \frac{\mu_0 I}{4\pi} \int_s d\boldsymbol{s} \times \frac{\boldsymbol{r}_{\mathrm{SF}}}{\|\boldsymbol{r}_{\mathrm{SF}}\|^3} \tag{25}$$

where I is the peak value of the current selected with 10 A, $\boldsymbol{r}_{\mathrm{SF}}$ the source-field-point vector, and s the integration path.

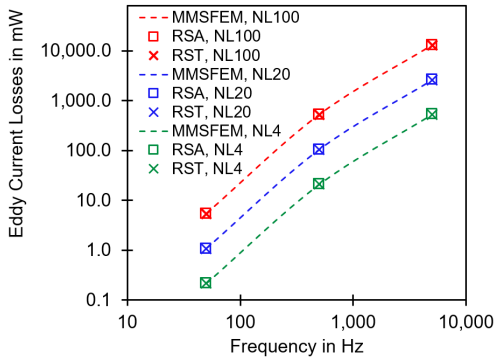

Fig. 4. Eddy-current losses of the entire problem for 4, 20, and 100 laminates denoted by NL4, NL20, and NL100, respectively.

To validate the results obtained by the MMSFEM, reference solutions have been computed with the SFEM using an $\boldsymbol{A}$ formulation (RSA) and the mixed $\boldsymbol{T}$, Φ–Φ formulation (RST). Second-order finite elements have been selected for $\boldsymbol{A}$ and $\boldsymbol{T}$ and the third-order ones for Φ, respectively. An analog selection has been made for the MMSFEMs.

To study the computational costs of the novel MMSFEM compared with reference solutions with respect to the number of laminates in the core, problems with 4, 20, and 100 laminates have been simulated. The finite-element model with four laminates of the MMSFEM uses two layers of finite elements in the z-direction, compared with Fig. 3, and the one with 20 laminates adds two layers representing 16 laminates. Finally, the model with 100 laminates adds further two layers for 80 laminates. Note that the number of laminates is increased by the factor of 5 from the SFEM model to the SFEM model, whereas the MMSFEM model grows with two finite-element layers in each case to emphasize the performance of the MMSFEM. Planes of symmetry are considered in all simulations. The same discretization by finite elements in the xy plane has been used in the models for the SFEM and MSFEM to ensure a fair comparison. Handmade hexahedral finite-element meshes have been made. To vary the penetration depth, the frequency was modified.

To avoid the development of a specific solver, all equation systems stemming either from an SFEM or from the MMSFEM have been solved by the direct solver PARDISO [13]. The higher order gradients have been eliminated from the finite-element spaces of $\boldsymbol{T}_h$ and $\boldsymbol{T}_{2h}$, respectively, using NGSolve [14].

B. Numerical Results

There is an excellent agreement between the reference solutions RST and RSA, respectively, and the MSFEM, as can easily be seen in Fig. 4 and by the relative error in Fig. 5. The average of the losses of RSA and RST has been used for the relative losses. The losses obtained by the MMSFEM are slightly smaller than the reference losses.

For the sake of transparency, all results are summarized in Table I.

C. Computational Costs

Numerical simulations show that the MMSFEM saves enormous computational costs with respect to the number of laminates compared with the corresponding SFEMs (see

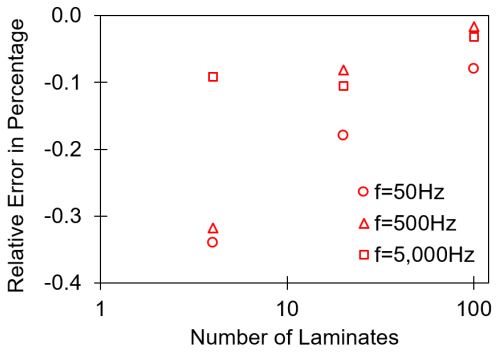

Fig. 5. Relative error of the eddy-current losses for 4, 20, and 100 laminates.

TABLE I
EDDY-CURRENT LOSSES IN mW OF THE ENTIRE PROBLEM

NL	f in Hz	RSA	RST	MMSFEM
4	50	0.2176	0.2197	0.2153
-	500	21.08	21.29	20.88
-	5,000	537.2	530.4	531.8
20	50	1.078	1.084	1.077
-	500	104.6	104.8	104.4
-	5,000	2,596	2,637	2,596
100	50	5.413	5.422	5.397
-	500	523.4	524.6	523.1
-	5,000	13,15	12,85	12,97

TABLE II
DEGREES OF FREEDOM

NL	f in Hz	RSA $\boldsymbol{A}$	RST $\boldsymbol{T}$	Φ	MMSFEM $\boldsymbol{T}_2$	Φ_0
4	500	233,235	30,628	71,630	28,295	60,610
-	5,000	289,977	68,350	163,731	-	-
20	500	687,171	153,140	192,270	41,276	70,180
-	5,000	970,881	341,750	436,427	-	-
100	500	2,956,851	765,700	795,470	67,238	89,320
-	5,000	4,375,401	1,708,750	1,799,907	-	-

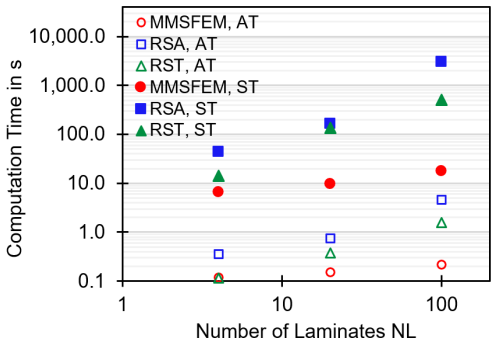

Fig. 6. Assembling time (AT) and solution time (ST) (Inverse Pardiso [13]).

Table II). For 5000-Hz simulations, the finite-element order of $\boldsymbol{T}$ and Φ has been increased to three and four, respectively, and the laminates have been split into two finite-element layers for the $\boldsymbol{A}$ formulation. Computation times are presented in Fig. 6, using a server with two times eight cores [Intel(R) Xeon(R) CPU 4110] and 192GB RAM. An MMSFEM is essentially faster than the reference solutions RSA and RST, respectively.

V. CONCLUSION

The presented MMSFEM is an attractive alternative to the MSFEM based on a magnetic vector potential $\boldsymbol{A}$ [4]. Contrary to the MSFEM with $\boldsymbol{A}$, considering the edge effect does not require an additional unknown. The edge effect is simply realized by prescribing the homogenous tangential Dirichlet boundary conditions of $\boldsymbol{T}_2$.

The novel MMSFEM requires only as many unknowns as a brute force simulation using $\boldsymbol{T}, \Phi$–Φ with an anisotropic conductivity in the first step, except that the MMSFEM provides the eddy currents due to the main magnetic field including the edge effect. In general, the savings of the MSFEM compared with RSA and RST grow clearly with the problem size measured by the number of laminates NL.

ACKNOWLEDGMENT

This work was supported by the Austrian Science Fund (FWF) under Project P 27028.

REFERENCES

[1] A. G. Jack and B. C. Mecrow, "Calculation of three-dimensional electromagnetic fields involving laminar eddy currents," *IEE Proc. A-Phys. Sci., Meas. Instrum., Manage. Educ.-Rev.*, vol. 134, no. 8, pp. 663–671, Sep. 1987.

[2] K. Preis, O. Bíró, and I. Ticar, "FEM analysis of eddy current losses in nonlinear laminated iron cores," *IEEE Trans. Magn.*, vol. 41, no. 5, pp. 1412–1415, May 2005.

[3] K. Hollaus and J. Schöberl, "Some 2-D multiscale finite-element formulations for the eddy current problem in iron laminates," *IEEE Trans. Magn.*, vol. 54, no. 4, Apr. 2018, Art. no. 7401716.

[4] K. Hollaus, "A MSFEM to simulate the eddy current problem in laminated iron cores in 3D," *COMPEL-Int. J. Comput. Math. Elect. Electron. Eng.*, vol. 38, no. 5, pp. 1667–1682, 2019.

[5] R. Albanese and G. Rubinacci, "Integral formulation for 3D eddy-current computation using edge elements," *IEE Proc. A-Phys. Sci., Meas. Instrum., Manage. Educ.-Rev.*, vol. 135, no. 7, pp. 457–462, Sep. 1988.

[6] T. Nakata, N. Takahashi, K. Fujiwara, and Y. Okada, "Improvements of the T-Ω method for 3-D eddy current analysis," *IEEE Trans. Magn.*, vol. MAG-24, no. 1, pp. 94–97, Jan. 1988.

[7] O. Bíró, "Edge element formulations of eddy current problems," *Comput. Methods Appl. Mech. Eng.*, vol. 169, nos. 3–4, pp. 391–405, 1999.

[8] O. Bottauscio, M. Chiampi, and D. Chiarabaglio, "Advanced model of laminated magnetic cores for two-dimensional field analysis," *IEEE Trans. Magn.*, vol. 36, no. 3, pp. 561–573, May 2000.

[9] P. Rasilo, E. Dlala, K. Fonteyn, J. Pippuri, A. Belahcen, and A. Arkkio, "Model of laminated ferromagnetic cores for loss prediction in electrical machines," *Electr. Power Appl.*, vol. 5, no. 7, pp. 580–588, Aug. 2011.

[10] M. Schöbinger, J. Schöberl, and K. Hollaus, "Multiscale FEM for the linear 2-D/1-D problem of eddy currents in thin iron sheets," *IEEE Trans. Magn.*, vol. 55, no. 1, Jan. 2019, Art. no. 7400212.

[11] P. Dular, "A time-domain homogenization technique for lamination stacks in dual finite element formulations," *J. Comput. Appl. Math.*, vol. 215, no. 2, pp. 390–399, 2008.

[12] O. Bottauscio, M. Chiampi, and A. Manzin, "Computation of higher order spatial derivatives in the multiscale expansion of electromagnetic-field problems," *IEEE Trans. Magn.*, vol. 44, no. 6, pp. 1194–1197, Jun. 2008.

[13] O. Schenk and K. Gärtner, *Pardiso*. Boston, MA, USA: Springer, 2011, pp. 1458–1464.

[14] J. Schöberl. *NetGen/NGSolve*. Accessed: Aug. 2019. [Online]. Available: https://ngsolve.org